Solid State Ionics 184 (2011) 47–51

Contents lists available at ScienceDirect

Solid State Ionics

journal homepage: www.elsevier.com/locate/ssi

Defect structure of the mixed ionic–electronic conducting Sr[Ti,Fe]O_x solid-solution system — Change in iron oxidation states and defect complexation

Michael D. Drahus, Peter Jakes, Emre Erdem, Rüdiger-A. Eichel *

Institut für Physikalische Chemie I, Universität Freiburg, Albertstr. 21, D-79104 Freiburg, Germany

ARTICLE INFO

Article history:
Received 4 June 2010
Received in revised form 24 September 2010
Accepted 24 September 2010
Available online 20 November 2010

Keywords:
Strontium titanate ferrite
Multi-valent iron
Oxygen vacancy
Charge compensation
Solubility limit

ABSTRACT

The oxidation/reduction behavior of iron in the Sr[$Ti_{1-y}Fe_y$]O_x solid-solution system, for $y \in [0.002; 0.05]$, under various oxygen partial pressures was examined through the use of electron paramagnetic resonance (EPR) spectroscopy. The results indicate that iron has been induced to move between di- tri- and tetravalent oxidation states. This results with the centers functioning as either a source (oxidation) or as a sink (reduction) for electrons. In particular it is shown that the reducibility of iron decreases with increasing iron content.

1. Introduction

The strontium titanate ferrite (Sr[Ti,Fe]O_x) solid-solution system is a *mixed ionic–electronic conductor*, with applications ranging from oxygen sensors [1–3] over fuel cells [4,5] to novel materials for resistive-switching memories based on a valency-change mechanism [6,7]. With this respect, the elucidation of defect structure plays a central role [8,9]. The most relevant defects are multivalent iron centers (Fe''_{Ti}, Fe'_{Ti}, $Fe^{\times}_{Ti}$, $Fe^{\bullet}_{Ti}$), oxygen vacancies ($V_O^{\bullet\bullet}$) and defect complexes between both, such as $(Fe''_{Ti}-V_O^{\bullet\bullet})^{\times}$ or $(Fe'_{Ti}-V_O^{\bullet\bullet})^{\bullet}$ for instance.

A good starting point to characterize the defect structure of the Sr[Ti,Fe]O_x solid-solution system, is to study Fe^{3+}-doped $SrTiO_3$ as one of the pure-member phases for varying iron dopant concentrations. The current understanding involves the iron functional center being incorporated as a trivalent ion on the titanium site, Fe'_{Ti}, when the iron is doped in low concentration [10]. Furthermore, for reason of charge compensation $(Fe'_{Ti}-V_O^{\bullet\bullet})^{\bullet}$ defect complexes are formed [11–15]. Both types of defects build a defect equilibrium

$$Fe'_{Ti} + V_O^{\bullet\bullet} \rightleftharpoons (Fe'_{Ti}-V_O^{\bullet\bullet})^{\bullet} \quad (1)$$

defining an equilibrium constant for defect association [16]

$$K_{ass} = \frac{[(Fe'_{Ti}-V_O^{\bullet\bullet})^{\bullet}]}{[Fe'_{Ti}][V_O^{\bullet\bullet}]} \quad (2)$$

that is a function of temperature and oxygen partial pressure. In a conclusive quantitative study of $(Fe'_{Ti}-V_O^{\bullet\bullet})^{\bullet}$ defect complexation in Fe-doped $SrTiO_3$ single crystals heat-treated under reduced oxygen partial pressure, K_{ass} has recently been determined [17]. However, this quantitative study only concerns trivalent iron centers, Fe'_{Ti} and $(Fe'_{Ti}-V_O^{\bullet\bullet})^{\bullet}$. Other oxidation states of the iron functional center that were earlier reported to exist for single-crystalline samples, such as $(Fe''_{Ti}-V_O^{\bullet\bullet})^{\times}$ [18], $Fe^{\times}_{Ti}$ [19] and $Fe^{\bullet}_{Ti}$ [20], were not considered.

Thus, in addition to the interaction of the iron functional center with oxygen vacancies impacting *ionic conduction*, we here aim to investigate the interaction of iron with electrons (*electronic conduction*), necessitating reactions that involve a change in oxidation state

$$Fe'_{Ti} + e' \rightleftharpoons Fe''_{Ti} \quad (3)$$

$$Fe'_{Ti} \rightleftharpoons Fe^{\times}_{Ti} + e' \quad (4)$$

As the *method-of-choice* for the study of paramagnetic functional centers, electron paramagnetic resonance (EPR) may be applied to characterize the defect structure [21,22].

2. Experimental

2.1. Sample synthesis

Iron doped samples of the concentration 0.2, 0.5, 1.0, 2.0 and 5.0 mol% Iron (B-Site cation ratio) were prepared using 100 nm strontium titanate (99.95%) powder from Inframat Advanced Materials as the starting material. Doping was accomplished by adding the appropriate amounts of $Fe(NO_3)_3$ (Aldrich 99.99%) and $Sr(NO_3)_2$ (Aldrich 99.995%) in an

* Corresponding author.
E-mail address: ruediger.eichel@physchem.uni-freiburg.de (R.-A. Eichel).

0167-2738/$ – see front matter © 2010 Elsevier B.V. All rights reserved.
doi:10.1016/j.ssi.2010.09.045

aqueous solution of the starting material and deionized water to achieve the desired iron concentration. The resulting mixture was sonically agitated, frozen with liquid nitrogen and subjected to freeze drying to remove the water. The resulting powder was calcined at 1200 °C in a muffle oven for 6 h under air atmosphere. Further heat treatment under controlled atmosphere conditions was carried out in a tube furnace at 1000 °C for 3 h under the flowing gas of the following atmospheres: O_2 (99.8%), Argon (99.999%), Ar (95%)/H_2 (5%), H_2 (99.95%). At the end of the heat treating time the furnace was shut off and allowed to cool to room temperature.

In order to ensure phase purity of the obtained samples, X-ray diffraction patterns were taken as depicted in Fig. 1. Clearly, the obtained patterns show pure cubic $SrTiO_3$ ($Pm\bar{3}m$), with lattice parameters of $a = 390.59(3)$ pm (1.0% Fe) and $a = 390.80(5)$ pm (5.0% Fe) as compared to undoped $SrTiO_3$ with $a = 390.50$ pm (ICDD [35–734]).

2.2. EPR spectroscopy

The X-band (9.8 GHz) EPR measurements were performed on a Bruker EMX spectrometer with an H_{011} cavity at ambient temperature. The magnetic field was read out with a NMR gaussmeter (ER 035M, Bruker) and as a standard field marker polycrystalline DPPH with $g = 2.0036$ was used for the exact determination of the resonance magnetic field values. For numerical spectrum simulation the EasySpin toolbox has been used [23].

3. Theory

For a theoretical description of the obtained EPR spectra, the spin-Hamiltonian concept is used [24]. The free trivalent iron ion possesses five unpaired electrons in the *3d*-shell ($3d^5$). As the orbital angular momentum is zero, the ground state of the ion is ${}^6S_{5/2}$ with $S = \frac{5}{2}$. In a crystal field, the Fe^{3+}-spin degeneracy is lifted into three Kramer's doublets due to internal electric field gradients. The remaining degeneracy may be lifted by an external magnetic field resulting in six Zeeman levels. The ^{57}Fe-hyperfine interaction has been neglected, as the only isotope with non-vanishing nuclear spin, ^{57}Fe ($I = \frac{1}{2}$), is present in only 2.1% natural abundance and was not observed in the recorded spectra. An effective spin-Hamiltonian may thus be written as

$$\mathcal{H} = \beta_e g \mathbf{B}_0 \cdot \mathbf{S} + \sum_{k=2,\ldots,2S}^{-k \le q \le k} B_k^q O_k^q(S_x, S_y, S_z) \tag{5}$$

in which the *g*-matrix is taken as isotropic with $g_e = 2.0023$ the free electron *g*-value, β_e denotes the Bohr magneton, $\mathbf{B}_0$ is the external magnetic field, B_k^q are the fine-structure Hamiltonian coefficients, and O_k^q are the extended Stevens spin operators [24]. The first term represents the electronic Zeeman interaction and the second term is the fine-structure Hamiltonian, describing the interaction of the crystal field with the paramagnetic Fe^{3+}-ion. The order *k* in the spin operators allows terms up to $k = 4$ for $S = \frac{5}{2}$.

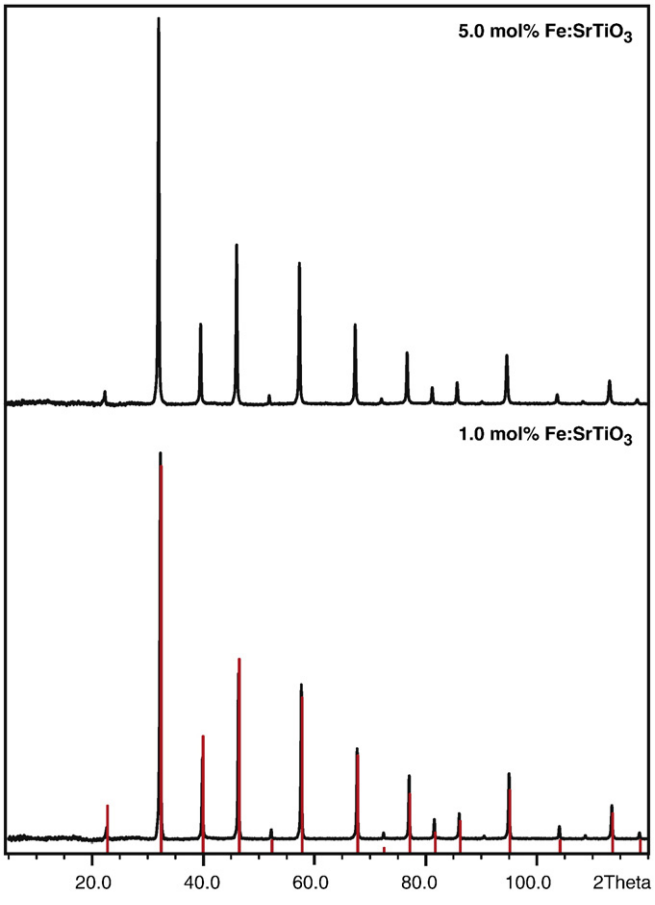

Fig. 1. Diffraction profiles for 1.0 mol% Fe^{3+} (bottom) and 5.0 mol% Fe^{3+}-doped $SrTiO_3$ (top) $SrTiO_3$ using $Cu_{K_{\alpha 1}}$-radiation ($\lambda = 154.0598$ pm) at ambient temperature.

4. Results and discussion

The corresponding EPR spectra of Fe^{3+}:$SrTiO_3$ as function of iron dopant concentration are shown in Fig. 2 (a). Obviously, the spectra are dominated by a strong resonance at $g = 2.001$. The small satellites are owing to 4th-order fine-structure interaction ($B_4^0 = 4.8$ MHz, $B_4^4 = 19.8$ MHz), for which reason the observed resonance is owing to *high-spin* Fe^{3+}. Because the 2nd-order fine-structure interaction parameters vanish ($B_2^0 = B_2^2 = 0$), the corresponding site-symmetry is cubic and the observed spectrum is due to acceptor-type Fe'_{Ti}.

The region at which typically the resonance for the $(Fe'_{Ti} - V_O^{\bullet\bullet})^{\bullet}$ defect complex occurs is displayed with enlarged magnification (factor 10). It may be described with $g = 2.001$ and $B_2^0 = 13.7$ GHz, thus being at an axial site symmetry. Clearly this signal, and thus the corresponding concentration $[(Fe'_{Ti} - V_O^{\bullet\bullet})^{\bullet}]$, is rather small as compared to the one for '*free*' Fe'_{Ti}. The spin-Hamiltonian parameters for both centers were refined by numerical spectrum simulation [23] and the corresponding parameters are summarized in Table 1. Exploiting values from literature, an obvious trend in *g*-values as function of iron oxidation state may be observed. Fe^{3+} with half-filled *3d*-shell has a *g*-value close to that of free electrons ($g_e = 2.0023$), whereas Fe^{2+} and Fe^{+} with more than half filled *3d*-shell have *g*-values smaller than g_e and Fe^{4+}, Fe^{5+} *g*-values larger than g_e [20].

A further experimental observation concerns the paramagnetic susceptibility, χ_{para}, of the different compounds that is analyzed by double integration of the c.w.-EPR spectra and comparison with a spin standard of known χ_{para}^{std}. With that respect, the obtained area is linear to the amount of Fe^{3+}. Because under the here applied experimental conditions the oxidation states Fe^{2+} and Fe^{4+} do not contribute the EPR susceptibility, the presence of Fe^{2+} and Fe^{4+} only indirectly manifests in terms of a line-broadening mechanism. Because the EPR spectrum of the $(Fe'_{Ti} - V_O^{\bullet\bullet})^{\bullet}$ defect complex extends over a comparatively broad range a rather broad spectrum has to be integrated and baseline corrected. Owing to this procedure, the main error is due to the baseline correction. Furthermore, when comparing with a spin standard an additional error occurs owing to differences in sample position in the resonator. Therefore *absolute* susceptibilities can only be obtained by a rather large uncertainty but *relative* susceptibilities are quite exact with an error in the range of ±5%.

Applying the above described procedure, the concentration of Fe^{3+} centers as function of $[Fe]_{total}$-dopant concentration may be obtained, as depicted in Fig. 3. Obviously, for the sample calcined under air atmosphere to a dopant concentration of 1.0 mol% the majority of iron

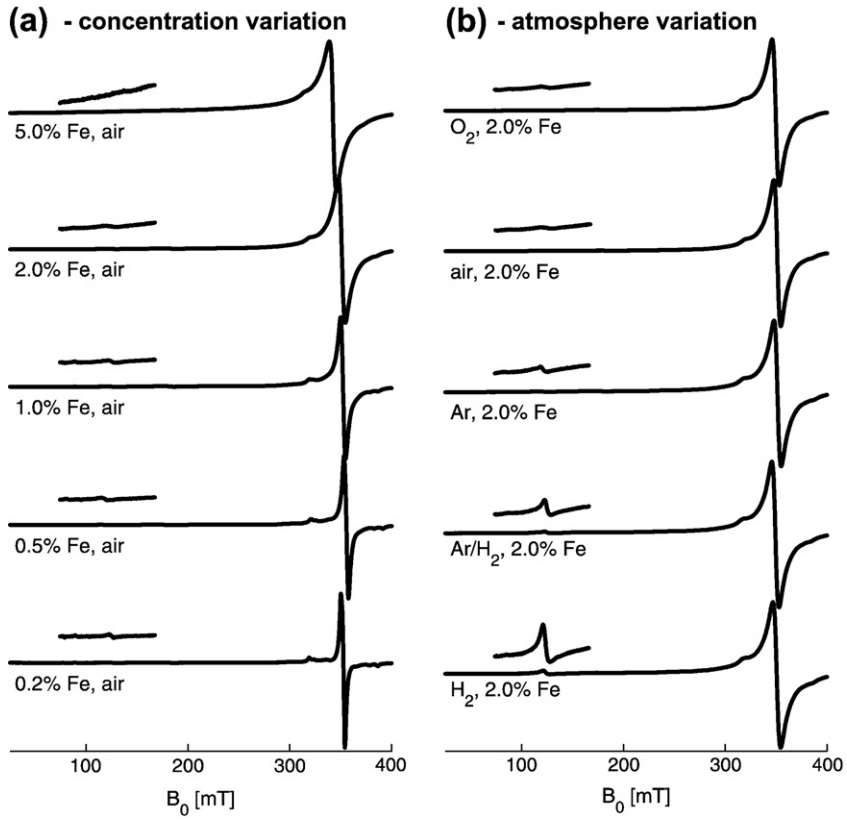

Fig. 2. X-band (9.8 GHz) EPR of Fe^{3+}-doped $SrTiO_3$ at ambient temperature. (a) variation of iron dopant concentration, $[Fe]_{total}$, calcined under air atmosphere. (b) effect of heat treatment under varying oxygen partial pressure, p_{O_2}, for 2.0 mol% Fe-doped $SrTiO_3$. The spectral region displaying the formation of $(Fe'_{Ti}-V_O^{\bullet\bullet})^{\bullet}$ defect complexes is plotted with enlarged magnification (factor 10). All spectra are normalized to identical maximum amplitude.

is incorporated as trivalent oxidation state. In this region, the electroneutrality condition has the form [17]

$$[Fe'_{Ti}] \approx 2[V_O^{\bullet\bullet}] \quad (6)$$

such that one $V_O^{\bullet\bullet}$ compensates two Fe'_{Ti} centers.

For higher dopant concentrations, the observed Fe^{3+} amount remains constant at about 1.0 mol%. Consequently, the additionally doped amount of iron has to be incorporated with an integer spin state, which is spectroscopically not observable with the here used low microwave frequencies (9.8 GHz). Such so-termed '*EPR-silent*' paramagnetic high-spin states would be Fe^{2+} ($3d^6$, $S=2$) or Fe^{4+} ($3d^4$, $S=2$) for instance. The corresponding condition for electroneutrality then changes into

$$[Fe'_{Ti}] + 2[Fe''_{Ti}] \approx 2[V_O^{\bullet\bullet}] \quad (7)$$

which involves an increase in relative amount of $V_O^{\bullet\bullet}$ per dopant iron, because in the divalent oxidation state one $V_O^{\bullet\bullet}$ compensates one Fe''_{Ti}-center.

Table 1
Spin-Hamiltonian parameters for different Fe-centers in $SrTiO_3$ as obtained after numerical spectrum simulation and compared to values from literature.

Center	g	B_2^0 [GHz]	B_4^0 [MHz]	B_4^4 [MHz]	Reference
$(Fe'''_{Ti}-V_O^{\bullet\bullet})'$	1.99	–	–	–	[18]
$(Fe''_{Ti}-V_O^{\bullet\bullet})^{\times}$	2.00	95.95	–	–	[18]
Fe'_{Ti}	2.001(5)	–	4.8(5)	19.8(5)	This work
	2.0	–	–	16.6	[10]
	–	–	–	–	
$(Fe'_{Ti}-V_O^{\bullet\bullet})^{\bullet}$	2.001(5)	13.7(5)	–	–	This work
	2.0	13.51	–	–	[10]
	2.008	14.27	–	–	[11]
	–	13.5	5	60	[11]
	2.010	13.52	–	–	[13]
	–	13.52	–	–	[14]
$Fe^{\times}_{Ti}$	2.007	–	–	188	[19]
$Fe^{\bullet}_{Ti}$	2.013	–	–	–	[20]

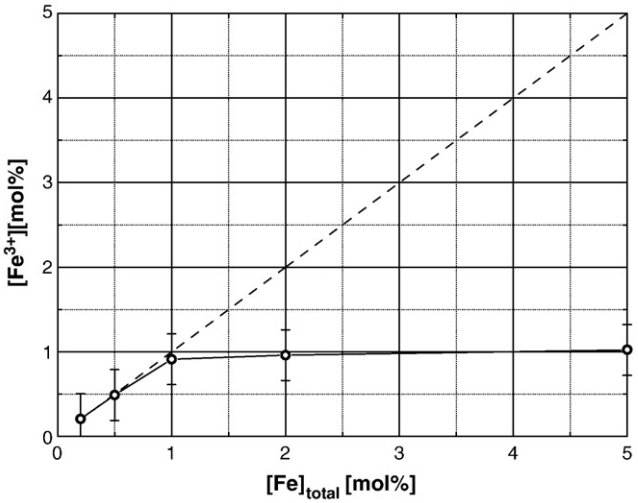

Fig. 3. Determined integral $[Fe'_{Ti}]$ and $[(Fe'_{Ti}-V_O^{\bullet\bullet})^{\bullet}]$-concentration, as function of $[Fe]_{total}$-dopant concentration for samples calcined under air-atmosphere. The dashed line indicates complete Fe^{3+} oxidation state, $[Fe^{3+}]=[Fe]_{total}$.

The thus determined upper limit for the Fe^{3+}-oxidation state in $SrTiO_3$ is in the order of 1.0 mol% for the samples calcined under air, which is similar to other perovskite compounds, such as Fe_2O_3-doped $Pb[Zr_{0.6}Ti_{0.4}]O_3$ [25] and Fe_2O_3-doped $[Bi_{0.5}Na_{0.5}]TiO_3$ [26]. However, different to the aforementioned systems, iron dopant concentrations above 1.0 mol% do not result in the formation of secondary phases, but rather involve changes in oxidation state according to Eqs. (3) and (4).

Moreover, a pronounced variation in EPR line width ΔB_{FWHM} for the Fe'_{Ti}-center as function of $[Fe]_{total}$-dopant concentration has been experimentally observed, as depicted in Fig. 4. This dependence may nicely be least-square fitted by a square-root dependence of the form

$$\Delta B_{FWHM}([Fe]_{total}) = \Delta B_{int} + B_{dip}\sqrt{[Fe]_{total}} \quad (8)$$

where ΔB_{int} is the natural intrinsic Fe^{3+} line width and B_{dip} a constant accounting for the Fe^{3+} spin–spin interaction [27,28]. Accordingly, ΔB_{FWHM} is mainly determined by electron spin–spin interaction and there is no observable impact of an exchange narrowing mechanism in the here studied dopant interval. Such mechanisms would have been expected if magnetic secondary phases exist for instance. Furthermore, the obtained line-width behavior is representative for homogeneously distributed Fe'_{Ti}-centers over the sample volume because any accumulation of the Fe'_{Ti}, for example at grain boundaries, would cause considerable deviation from the observed line-width dependence. Exploiting the inverse proportionality between ΔB_{FWHM} and the electron spin–spin relaxation time T_2, these may be determined spanning a range $T_2 \in [1; 10]$ ns.

Finally, the oxygen partical pressure, p_{O_2}, has been varied during high-temperature processing for a 0.5 and a 2.0 mol% Fe-doped $SrTiO_3$ sample (cf. Fig. 5). In none of the spectra heat-treated under reducing atmosphere the formation of trivalent titanium Ti'_{Ti} [29] or $(Ti'_{Ti} - V_O^{\bullet\bullet})^{\bullet}$ defect complexes [30] has been observed.

Starting from a normalized amount of Fe^{3+} for both samples calcined under air atmosphere, a pronounced increase in $[Fe'_{Ti}]$ is observed for the 2.0 mol% Fe-doped $SrTiO_3$ sample for decreasing p_{O_2} (cf. Fig. 5). Correspondingly a change in iron oxidation-state occurs according to

$$Fe_{Ti}^{\times} + e' \rightarrow Fe'_{Ti} \quad (9)$$

such that part of the '*EPR-silent*' Fe^{4+} is converted into observable Fe^{3+}. Contrary, the amount of Fe^{3+} remains almost unchanged for the 0.5 mol% Fe-doped compound.

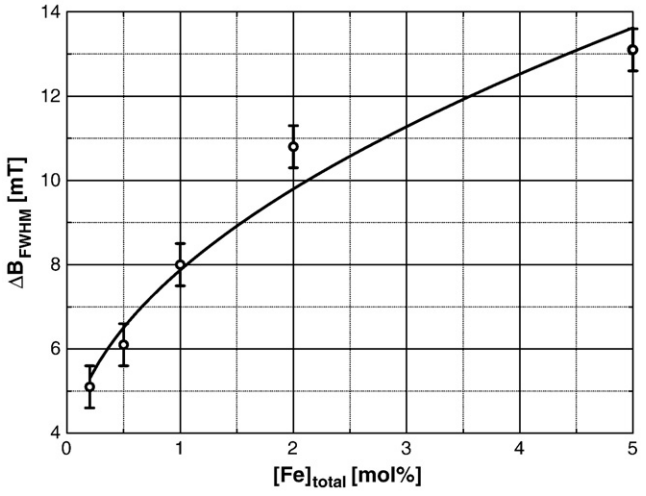

Fig. 4. Determined variation in EPR line width ΔB_{FWHM} for the Fe'_{Ti}-center as function of $[Fe]_{total}$-dopant concentration. The experimental values are least-square fitted using Eq. (8).

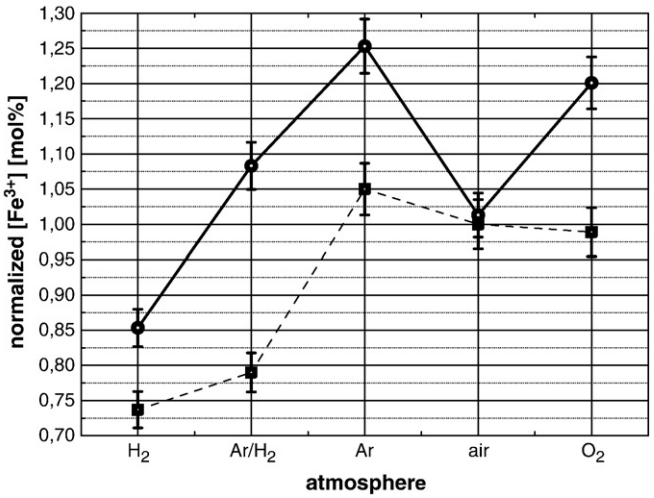

Fig. 5. Determined integral $[Fe'_{Ti}]$ and $[(Fe'_{Ti} - V_O^{\bullet\bullet})^{\bullet}]$-concentration for 0.5 (bottom) and 2.0 mol% (top) Fe^{3+}-doped $SrTiO_3$, as function of heat-treatment under varying oxygen partial pressures. For reason of comparability, the $[Fe^{3+}]$-concentrations were normalized to the corresponding concentrations under air.

When further reducing p_{O_2}, a decrease in $[Fe'_{Ti}]$ occurs for both samples. This observation may be explained by an iron oxidation-state change owing to

$$Fe'_{Ti} + e' \rightarrow Fe''_{Ti} \quad (10)$$

where part of the Fe^{3+} is converted into '*EPR-silent*' Fe^{2+}.

On the other hand, when increasing p_{O_2} the samples with 0.5 and 2.0 mol% Fe-doping behave differently. Whereas the amount of Fe^{3+} in the 0.5 mol% Fe-doped $SrTiO_3$ compound marginally decreases, the Fe^{3+}-concentration increases for the 2.0 mol% Fe-doped sample. Accordingly, in the latter case the following oxidation reaction is expected to take place

$$Fe''_{Ti} \rightarrow Fe'_{Ti} + e' \quad (11)$$

Consequently, part of the '*EPR-silent*' Fe^{2+} are transferred to Fe^{3+}-centers, reversing the reduction reaction (10).

The observed difference in the reduction/oxidation behavior as function of Fe-doping level can be explained as follows: because for the 0.5 mol% Fe-doped $SrTiO_3$ sample calcined under air almost all iron is in the trivalent Fe^{3+} oxidation state, there is only vanishing amount of Fe^{4+} and Fe^{2+} present for change in oxidation state according to Eqs. (9) and (11). This situation is clearly different for the 2.0 mol% Fe-doped compound, where prominent concentrations of Fe^{4+} and Fe^{2+} are present (cf. Fig. 3), such that the initial Fe^{3+}-concentration may be enhanced by reduction and oxidation reactions (9) and (11).

The e' occurring in Eqs. (9)–(11) are generated or annihilated by the following oxygen non-stoichiometry equilibrium that is shifted as a function of p_{O_2}

$$O_O^{\times} \rightleftharpoons V_O^{\bullet\bullet} + 2e' + \frac{1}{2}O_2(g) \quad (12)$$

Exploiting the oxidation–reduction reactions (9)–(11), above 1.0 mol% of iron doping, the following equilibrium has to be present

$$2Fe'_{Ti} \rightleftharpoons aFe''_{Ti} + bFe_{Ti}^{\times} + ce' \quad (13)$$

with equilibrium constant

$$K_{redox} = \frac{[Fe''_{Ti}]^a [Fe_{Ti}^{\times}]^b [e']^c}{[Fe'_{Ti}]^2} \quad (14)$$

The here described situation is consistent with the proposed defect chemistry after which the reducibility of iron in Sr[Ti,Fe]O_x increases with $[Fe]_{total}$ [3].

In addition to the valence-change reactions (9)–(11) of the iron functional centers, they also interact with ionic charge carriers ($V_O^{\bullet\bullet}$) when reducing p_{O_2} (cf. Fig. 2 (b)) by forming defect complexes according to Eq. (1) [17]. Owing to the fact that in some specimen $[Fe''_{Ti}]$ may also be present, which is spectroscopically not observable under the here used conditions ('*low-frequency regime*'), we also expect the formation of electrically neutral $(Fe''_{Ti}-V_O^{\bullet\bullet})^{\times}$ defect complexes, as it has been shown that it is a characteristic property of acceptor-type centers in perovskite oxides to form defect complexes with oxygen vacancies [31]. Examples include electrically neutral $(Cu''_{Ti}-V_O^{\bullet\bullet})^{\times}$ in $PbTiO_3$ [32,33], $(Mn''_{Ti}-V_O^{\bullet\bullet})^{\times}$ in $SrTiO_3$ [14,34] and in $BaTiO_3$ [35], as well as mutually compensating charged $(Cu'''_{Nb}-V_O^{\bullet\bullet})'$ and $(V_O^{\bullet\bullet}-Cu'''_{Nb}-V_O^{\bullet\bullet})^{\bullet}$ defect complexes in $[K_yNa_{1-y}]NbO_3$ [36].

5. Conclusion and outlook

In summary, it has been seen by EPR that in the oxygen partial pressure range used in this experiment the iron can be induced to move between the oxidation states of +2, +3 and +4. In doing so, it either behaves as a source (*oxidation*) or a sink (*reduction*) for electrons.

Further experiments will be aimed at the determination of the reduction enthalpy under different doping concentrations and oxygen partial pressures. Moreover, high-frequency EPR shall be applied in order to unambiguously prove the existence of Fe^{2+} and Fe^{4+} oxidation states.

Acknowledgments

This research has been financially supported by the DFG centre of excellence 595 'Electrical Fatigue in Functional Materials'. The support of Dr. Martin Ade and Prof. Stefan Weber to this research is acknowledged.

References

[1] A. Rothschild, S.J. Litzelman, H.L. Tuller, W. Menesklou, T. Schneider, E. Ivers-Tiffee, Sensors Actuators B 108 (2005) 223–230.
[2] S.J. Litzelman, A. Rothschild, H.L. Tuller, Sensors Actuators B 108 (2005) 231–237.
[3] A. Rothschild, W. Menesklou, H.L. Tuller, E. Ivers-Tiffee, Chem. Mater. 18 (2006) 3651–3659.
[4] E. Chinarro, J.C. Perez, B. Moreno, M. Carrasco, J.R. Jurado, in: N. Sammes, et al., (Eds.), Full Cell Technologies - State and Perspectives, 2005, pp. 187–192.
[5] W.C. Jung, H.L. Tuller, J. Electrochem. Soc. 155 (2008) B1194–B1201.
[6] R. Waser, M. Aono, Nat. Mater. 6 (2007) 833–840.
[7] R. Waser, R. Dittmann, G. Staikov, K. Szot, Adv. Mat. 21 (2009) 2632–2663.
[8] N.H. Chan, R.K. Sharma, D.M. Smyth, J. Electrochem. Soc. 128 (1981) 1762–1768.
[9] R. Merkle, J. Maier, Angew. Chem. Int. Ed. 47 (2008) 3874–3894.
[10] R.G. Pontin, E.F. Slade, D.J.E. Ingram, J. Phys. C 2 (1969) 1146–1150.
[11] E.S. Kirkpatrick, K.A. Müller, R.S. Rubins, Phys. Rev. 135 (1964) A86–A90.
[12] R. Baer, G. Wessel, R.S. Rubins, J. Appl. Phys. 39 (1968) 23–28.
[13] T. von Waldkirch, K.A. Müller, W. Berlinger, Phys. Rev. B 5 (1972) 4324–4334.
[14] E. Siegel, K.A. Müller, Phys. Rev. B 19 (1979) 109–120.
[15] H. Mestric, R.-A. Eichel, T. Kloss, K.P. Dinse, S. Laubach, P.C. Schmidt, K.A. Schönau, M. Knapp, H. Ehrenberg, Phys. Rev. B 71 (2005) 134109.
[16] D.M. Smyth, The Defect Chemistry of Metal Oxides, Oxford University Press, New York, 2000 Chap. 5.
[17] R. Merkle, J. Maier, Phys. Chem. Chem. Phys. 5 (2003) 2297–2303.
[18] R. Berney, D. Cowan, F. Morin, Solid State Commun. 26 (1978) 579–582.
[19] O.F. Schirmer, W. Berlinger, K.A. Müller, Solid State Commun. 16 (1975) 1289–1292.
[20] K.A. Müller, T. von Waldkirch, W. Berlinger, B.W. Faughnan, Solid State Commun. 9 (1971) 1097–1101.
[21] R.-A. Eichel, J. Electroceram. 19 (2007) 9–21.
[22] R.-A. Eichel, Phys. Chem. Chem. Phys. (2010), doi:10.1039/B918782K.
[23] S. Stoll, A. Schweiger, J. Magn. Reson. 178 (2006) 42–55.
[24] A. Abragam, B. Bleaney, Electron paramagnetic resonance of transition ions, Clarendon Press, Oxford, 1970.
[25] H.J. Kleebe, S. Lauterbach, L. Silvestroni, H. Kungl, M.J. Hoffmann, E. Erdem, R.-A. Eichel, Appl. Phys. Lett. 94 (2009) 142901.
[26] E. Aksel, E. Erdem, P. Jakes, J.L. Jones, R.-A. Eichel, Appl. Phys. Lett. 97 (2010) 012903.
[27] C.P. Poole, Electron Spin Resonance, 2nd ed.Dover Publications, New York, 1983.
[28] C.P. Slichter, Principles of Magnetic Resonance, 3rd ed.Springer, Heidelberg, 1996.
[29] R. Scharfschwerdt, A. Mazur, O.F. Schirmer, H. Hesse, S. Mendricks, Phys. Rev. B 54 (1996) 15284.
[30] E. Erdem, P. Jakes, R.-A. Eichel, D.C. Sinclair, M. Pasha, I.M. Reaney, Funct. Mat. Lett. 3 (2010) 65–68.
[31] P. Erhart, R.-A. Eichel, P. Träskelin, K. Albe, Phys. Rev. B 76 (2007) 174116.
[32] R.-A. Eichel, P. Erhart, P. Träskelin, K. Albe, H. Kungl, M.J. Hoffmann, Phys. Rev. Lett. 100 (2008) 095504.
[33] R.-A. Eichel, M.D. Drahus, P. Jakes, E. Erünal, E. Erdem, S.K.S. Parashar, H. Kungl, M.J. Hoffmann, Mol. Phys. 107 (2009) 1981–1986.
[34] R.A. Serway, W. Berlinger, K.A. Müller, R.W. Collins, Phys. Rev. B 16 (1977) 4761–4768.
[35] L.X. Zhang, E. Erdem, X. Ren, R.-A. Eichel, Appl. Phys. Lett. 93 (2008) 202901.
[36] R.-A. Eichel, E. Erünal, M.D. Drahus, D.M. Smyth, J. van Tol, J. Acker, H. Kungl, M.J. Hoffmann, Phys. Chem. Chem. Phys. 11 (2009) 8698–8705.